Published in final edited form as:
*Ultrasound Med Biol*. 2008 June ; 34(6): 902–912. doi:10.1016/j.ultrasmedbio.2007.11.020.

# NONINVASIVE ULTRASOUND ELASTICITY IMAGING (UEI) OF CROHN'S DISEASE: ANIMAL MODEL

**Kang Kim**[*], **Laura A. Johnson**[†], **Congxian Jia**[*], **Joel C. Joyce**[†], **Sujal Rangwalla**[†], **Peter D. R. Higgins**[†], and **Jonathan M. Rubin**[‡]

[*]Department of Biomedical Engineering, University of Michigan, Ann Arbor, MI, USA

[†]Department of Internal Medicine, University of Michigan, Ann Arbor, MI, USA

[‡]Department of Radiology, University of Michigan, Ann Arbor, MI, USA

## Abstract

Inflammation occurs in episodic flares in Crohn's disease, which are part of the waxing and waning course of the disease. Healing between flares allows the intestine to reconstitute its epithelium, but this healing results in the deposition of fibrotic scar tissue as part of the healing process. Repeated cycles of flares and healing often lead to clinically significant fibrosis and stenosis of the intestine. Patients are treated empirically with steroids, with their many side effects, in the hope that they will respond. Many patients would be better treated with surgery if we could identify which patients truly have intestinal fibrosis. Ultrasound elasticity imaging (UEI) offers the potential to radically improve the diagnosis and management of local tissue elastic property, particularly intestinal fibrosis. This method allows complete characterization of local intestine tissue with high spatial resolution. The feasibility of UEI on Crohn's disease is demonstrated by directly applying this technique to an animal model of inflammatory bowel disease (IBD). Five female Lewis rats (150 –180*g*) were prepared with phosphate buffered solution (PBS) as a control group and six were prepared with repeated intrarectal administration of trinitrobenzenesulfonic acid (TNBS) as a disease group. Preliminary strain measurements differentiate the diseased colons from the normal colons ($p < 0.0002$) and compared well with direct mechanical measurements and histology ($p < 0.0005$). UEI provides a simple and accurate assessment of local severity of fibrosis. The preliminary results on an animal model also suggest the feasibility of translating this imaging technique directly to human subjects for both diagnosis and monitoring.

### Keywords

Ultrasound elasticity imaging; Strain imaging; Nonlinear tissue elasticity; Crohn's disease

## INTRODUCTION

Intestinal fibrosis is a common result of cycles of inflammation and healing in Crohn's disease. Inflammation occurs in episodic flares in Crohn's disease, and these flares are part of the waxing and waning course of inflammatory bowel disease (IBD) (Loftus et al. 2002). The healing phase between flares allows the intestine to reconstitute its basement membrane and epithelium, but results in the deposition of fibrotic scar tissue as part of the healing process. The net result of such changes should lead to an alteration of the elastic properties



Address correspondence to: Dr. Kang Kim, Department of Biomedical Engineering, University of Michigan, 2200 Bonisteel Blvd., Ann Arbor, MI 48109. kangkim@umich.edu.

of the intestine as has been documented for other tissues (Krouskop et al. 1998). Fibrous changes of the intestine may become excessive over time in certain regions and this ultimately produces colon strictures. Patients, despite intensification in antiinflammatory medical therapy over the past 75 years, continue to progress from inflammatory symptoms to a structuring phenotype, and eventually to fistulizing disease (Louis et al. 2001).

Repeated cycles of flares and healing often lead to clinically significant fibrosis and stenosis of the intestine, requiring surgery in 20% of patients within three years of diagnosis (Sands et al. 2003). Intestinal surgery was eventually required in as many as 57% of patients in a 30-year cohort study in Olmsted County, Minnesota (Silverstein et al. 1999). Surgical resection of the intestine produces substantial personal and economic impact (Feagan et al. 2000), but the currently available treatments for Crohn's disease are directed at controlling inflammation without slowing or preventing fibrosis (Froehlich et al. 2005). When Crohn's patients have abdominal pain and vomiting, this often indicates severe narrowing of the small intestine. This can be because of inflammation, which can be treated with medical therapy, or because of chronic fibrosis, which requires surgery. Although we can identify inflammation with computed tomography (CT) scanning, we cannot identify which patients have significant intestinal fibrosis. Patients are treated empirically with steroids, with their many side effects, in the hope that they will respond. Many patients would be better treated with surgery if we could identify which patients truly have severe intestinal fibrosis causing their intestinal strictures.

Ultrasound imaging has been applied extensively toward assessing Crohn's disease. These applications have included assessment of bowel wall thickness, bowel wall vascularity using color or power Doppler with or without contrast agents and assessments for the presence of fistulae or regional lymph node involvement (Fraquelli et al. 2005; Kratzer et al. 2005; Maconi et al. 2005). It is clear that the bowel wall increases in thickness with Crohn's disease, although this thickening may not be reflective of the activity of the disease (Mayer et al. 2000; Robotti et al. 2004; Maconi et al. 2006). However, vascularity estimates seem to correspond to disease activity, and this may be a way to detect active disease (Sallomi 2003; Di Sabatino et al. 2004; Parente et al. 2004; Kratzer et al. 2005). It is hoped that one could then infer the degree of fibrosis based on the relative lack of vascularity in involved bowel segments (Di Sabatino et al. 2004; Parente et al. 2005; Maconi et al. 2006). Yet, none of these methods will directly evaluate the degree of fibrosis.

One potential technique to assess mechanical property change in the intestine because of the fibrosis development in the process of the repeated cycles of flares and healing is ultrasound elasticity imaging (UEI).

UEI has been found to be a valuable noninvasive tool to investigate mechanical characteristics of biological tissue (Lerner et al. 1988; Ophir et al. 1991, Ophir et al. 1996; Skovoroda et al. 1994; Hall et al. 2001). It relies on accurate estimates of tissue motion (speckle tracking) between two frames before and after deformation of the tissue. In UEI the excitation is produced by actually pushing on tissue with an ultrasound transducer itself, and recording the tissue deformation with real-time ultrasound images (Ophir et al. 1991; Sarvazyan et al. 1990). This constitutes a near static deformation with an external force. Other researchers have explored combinations of static or dynamic deformations with internal or external surface forces to induce deformations (Kim et al. 2004; Lerner et al. 1990). To date, no definitive studies have shown which deformation technique is superior for all applications. Speckle tracking was introduced initially in 1-D to estimate tissue motion along the axial direction (the beam propagation direction) (Ophir et al. 1991 and Downing et al. 1996) and has been expanded into 2-D with the development of the current 2-D ultrasound imaging systems. Two-dimensional speckle tracking measures displacements

of a speckle pattern in both axial and lateral (perpendicular to the beam direction in the imaging plane) dimensions (Geiman et al. 2000; Konofagou et al. 1998; Insana et al. 1998; Lubinski et al. 1996 and Browse et al. 1999). The most commonly used elasticity imaging techniques are based on 2-D correlation-based speckle tracking methods (Konofagou et al. 1998; Insana et al. 1998; Lubinski et al. 1996 and 1999). Speckle displacements are estimated from correlation lags corresponding to the maximum correlation coefficient between the frames. In the past decade, elasticity imaging based on speckle tracking has been shown to be a great potential for clinical uses (Lerner et al. 1988; Tristam et al. 1988; Bertrand et al. 1989; Yamakoshi et al. 1990; Sarvazyan et al. 1990; O'Donnell et al. 1991; Ophir et al. 1991; Ryan et al. 1992; Gao et al. 1996; Bilgen et al. 1996), where several groups have also explored high spatial resolution ultrasound speckle tracking systems for intravascular applications (O'Donnell et al. 1991; Ryan et al. 1992; Shapo et al. 1995; Emelianov 1998a; van der Steen et al. 1998; de Korte et al. 1998; Choi et al. 1999; Rekhter et al. 1999). UEI has also been successfully applied to other *in-vivo* applications. These include thrombus aging/maturational evaluation in human lower limb deep venous thrombosis (DVT) (Rubin 2003, Rubin 2006), breast cancer diagnosis (Garra 1997; Hall 2003), differentiation of benign and malignant thyroid masses (Lyshchik 2005), differentiation of benign and malignant cervical lymph nodes (Lyshchik 2007), prostate cancer detection (Cochlin 2002; Lorenz 1999), renal transplant graft nephropathy evaluation(Weitzel 2004), characterization of arterial wall stiffness for early atherosclerosis diagnosis (Kim 2004; Weitzel 2005), assessment of myocardial wall stiffness for detection of contractile dysfunction (Perk 2007), atheromata assessment for determining vulnerable plaque (Baldewsing 2007), assessment of the degree of liver fibrosis (Ziol 2005; Castera 2005; de Franchis 2007; Emelianov 1998b) and breast cancer screening (Booi et al. 2005, Booi et al. 2006).

In this study, the feasibility of UEI on Crohn's disease is demonstrated by directly applying this technique to an animal model of IBD, first described by Morris (1989) (PMID 2914642). UEI consists of combining two procedures: (i) application of controlled deformation of the study object and (ii) phase-sensitive, 2-D ultrasound speckle tracking and evaluation of internal tissue motion, *i.e.*, measurement of displacement and strain components. Preliminary strain measurements differentiate the diseased colons from the normal colons and compare well with direct mechanical measurements and histology.

## MATERIALS AND METHODS

### Animal model

Repeated intrarectal administration of 2,4,6-trinitrobenzenesulfonic acid (TNBS) in rats is a well-characterized animal model of intestinal colitis and fibrosis, first described by Morris (1989) (PMID 2914642). The protocol was approved by the University of Michigan Committee on the Use and Care of Animals and strictly complied with the National Institutes of Health Guide for the Care and Use of Laboratory Animals. A total of 11 female Lewis rats (Harlan Sprague-Dawley, Inc., IN, 150–180*g*) were studied. They were separated into two studies with five rats in the first study and the remaining six in the second. Study 1 included two control rats and three TNBS treated rats, and study 2 consisted of three control rats and three TNBS-treated rats. The animal preparation procedures described below were similar. Two groups were studied at different times.

The rats were fasted for 16 to 24 h and provided with an iso-osmotic bowel preparation solution (Golytely) to eliminate stool in the colon before intracolonic administration of TNBS by enema. Rats were anesthetized with inhaled isoflurane using the drop jar technique. Rats were placed in an inverted position and a 5 French feeding tube was inserted 6 cm into the animal's rectum to slowly instill 250 μL of either TNBS solution or a control

solution of phosphate-buffered saline solution (PBS). The enema tube remained in the rectum for 1 min to ensure adequate delivery to the left colon. The TNBS solution was made by diluting TNBS to a final concentration of 15 mg in 250 μL in a 50% ethanol. In this method, ethanol functions as the “barrier breaker” to permeabilize the mucosa of the left colon while TNBS acts as a hapten, attaching to submucosal proteins in the left colon. This haptenization of colonic proteins induces colonic inflammation and ulceration. Weekly escalating doses of 15 up to 60 mg TNBS induced inflammation and reproduced the cycle of inflammation, mucosal healing and eventual fibrosis characteristic of human IBD (Lawrance et al. 2003). During the weekly treatment phase, rats were monitored for weight loss, stool consistency, stool blood and general health. After five to eight TNBS treatment cycles, TNBS treatment was discontinued one week before euthanasia to allow resolution of inflammation. The animals were euthanized by $CO_2$ inhalation and the colon was excised, longitudinally opened and rinsed with saline before determining weight and length. The colon was photographed and scored for gross appearance of inflammation, necrosis and fibrosis. Representative sections of unaffected proximal or fibrotic distal colon were excised for histology, RNA and protein analysis. Chronic TNBS dosing produced a fibrotic response, specifically in the last 6 cm of the distal left colon, whereas proximal right colon sections were unaffected, thus providing an intra-animal control for fibrosis. The initial TNBS experiment (study 1) followed an eight-week TNBS treatment cycle of escalating weekly TNBS dosing from 15 to 60 mg. To reduce the risk of mortality, the subsequent experiment (study 2) followed a five-week TNBS course with dosing from 15 to 45 mg.

### Ultrasound RF data capturing

Ultrasound RF data were recorded using a commercial ultrasound scanner (iU22, Philips, Bothell, WA, USA) with a linear array transducer (L12–5, Philips) centered at 6.8 MHz. Before ultrasound analysis, animals were anesthetized with ketamine (40 mg/kg)/xylazine (4 mg/kg), IM. Anesthetized rats on the day of planned euthanasia were placed on a custom-built platform in a supine position with the abdomen exposed to the transducer (Fig. 1). The imaging transducer was also served to compress the rat’s abdominal wall and underlying tissue. The abdomen was shaved before imaging. The ultrasound transducer was fixed to a laboratory designed deformation device to induce a uniform displacement. The RF frames were captured at a rate of 49 Hz while about 10 to 20% average strain was being generated over 6 s. Overall experimental setup is similar to the previous study with DVT aging study (Xie et al. 2004, 2005).

When ultrasound imaging, transverse views of the cecum and bowel were carefully interrogated to insure accurate positioning of the transducer on the rat’s colon (Fig. 2). The regions-of-interest (ROI) were localized in the transverse orientation by first localizing the symphysis pubis. This is easy to recognize as an inverted U-shaped bony structure at the lower pelvis. We then moved the ultrasound probe proximally until the bony landmark disappeared and the sound penetrated into the abdomen. The distal sigmoid colon was imaged at this position. The colon was often filled with bowel contents and gas. These could be identified as being highly echogenic while producing a distal shadow. The gas and bowel contents could be pushed out of the section by preloading the section sufficiently to collapse the bowel walls, but not deform them. A second image of the rectum/distal sigmoid colon was routinely obtained. This was generated by manually moving the rat’s body 1 cm caudally while imaging the loop of bowel of interest in the transverse orientation. After 1 cm displacement, the next deformation was performed. We selected 1 cm because the elevational focal width is <1 cm, so these images would be independent. Finally, as an internal control, we imaged a segment of bowel that was at least 7 cm proximal to the rectum. This bowel was proven to be uninvolved with the therapeutic maneuvers.

Once the appropriate site was localized, a mild preload force was exerted to deform the abdomen in the transverse plane to reduce shadowing artifacts and the strain absorbing effects of fluid or gas-filled bowel. This preloading force completely collapsed any normal overlying bowel visible on the gray scale ultrasound image. This relatively mild preloading will not affect the elastic property of the colon wall as the bowel with its gas and liquid contents are very compliant; orders of magnitude more compliant than the surrounding soft-tissue, which is essentially incompressible. This is a reasonable assumption based on the fact that bowel is a very long, thin walled, open tube containing mainly gas and liquid. Hence, even modest pressure on the abdominal surface will immediately and preferentially collapse the normal bowel by forcing the luminal gas and liquid contents out of the imaging section. The investigators started the deformation at this minor preload stage. For each 6-s deformation, typically 294 frames of ultrasound RF data were collected in real time while the abdomen was being deformed. For each rat, three different transverse planes were imaged along the colon length. To guarantee independent measurements, these planes were separated by at least the elevational beamwidth (on the order of 1–2 mm) of the point spread function; two planes (distal) 1 cm apart in the sigmoid colon immediately above the symphysis pubis and one plane at least 7 cm proximal in the neighborhood of the cecum. For some of the cecal measurements (two out of three on the average), the bowel would translate out of the imaging frame during the deformation. To avoid this eventuality, the operator performing the deformation (JMR) would constrain the two sides of the abdomen with the thumb and forefingers of his left hand to prevent the bowel from translating laterally out of the frame. The mild preloading generated by this maneuver will be mostly absorbed by subcutaneous and mesenteric fat and will not be transferred to the small colon. The region immediately adjacent to cecum is always considered to be normal. The imagers (KK, CJ, JMR) were not informed about the treatment status (TNBS *vs.* PBS placebo) of each rat.

## Strain estimates

Collected RF data were processed off-line. Phase-sensitive correlation-based 2-D speckle tracking algorithm was applied to determine the in-plane frame-to-frame displacement (Lubinski et al. 1999). Frame-to-frame axial and lateral displacements were estimated from the position of the maximum correlation coefficient from the cross-correlation on the baseband complex signals. The correlation kernel size was set to be equal to about the speckle spot (250 μm in axial by 500 μm in lateral direction) for optimal strain estimation with minimum displacement (time delay) estimation variance (Lubinski et al. 1999). Axial displacements were then refined using the phase zero-crossing of the complex correlation function. A spatial filter, which was twice as big as the kernel size, was used to enhance the signal-to-noise ratio with reasonable spatial resolution. Frame-to-frame displacement estimates were then integrated from and registered to the initial coordinate system (*i.e.*, Lagrangian presentation). Spatial derivatives of the displacements were computed to produce radial normal strain (*i.e.*, the radial derivative of the radial displacement). In the rest of this paper, the radial normal strain will be called simply the strain where appropriate. To account for variable deformation force across different rats and different scan regions, strain needs to be normalized. Given the fact that the material between the spine/posterior body wall and bowel loops as well as the relative positions are consistent among all rats, we hypothesize that spine/posterior body wall displacement is suitable for normalization. Therefore, strain images were normalized individually by the magnitude of the average applied strain (10–20% in this study) estimated by estimating the displacement of the spine or posterior body wall during each deformation. The normalized strain can be any nonpositive number. If the normalized strain is less than −1, the colon is softer than its surrounding tissue on average. The bowel wall of interest was identified as a hypoechogenic closed curve located between the hyperechogenic luminal bowel contents and the surrounding soft tissue.

### Direct mechanical measurements

After the ultrasound imaging, animals were euthanized with inhaled $CO_2$. The entire colon was excised and rinsed with PBS. The colon tissue was dissected into 1 cm by 1 cm pieces for a direct mechanical measurement. The thickness of the samples ranges from 1.0 mm to 4.0 mm. The colon sections for mechanical measurement were immediately placed into the elastometer device (MicroElastometer, Artann Laboratories, Lamberville, NJ, USA), which is shown in Fig. 3. The compression force is measured by a strain gage (Acculab VI-200, Acculab) mounted under the object plate. The measurable force range is up to 2N with a precision of 0.1 mN. The MicroElastometer employs a pressing stamp with a rectangular cross-section of 8.88 mm by 3.98 mm. The position of the compression stamp is controlled by a hybrid linear actuator (HIS 35N67–12 to 405). The minimum travel distance per step is 3 μm. The MicroElastometer uses a bidirectional RS-232 interface to communicate with the user's computer through serial and parallel ports. Its software is a Windows (Microsoft, Redmond, WA, USA) application. The detailed specification can be found in the previous study on DVT (Xie et al. 2005). The MicroElastometer measures the displacement *vs.* force while a test tissue sample is subjected to compression. Based on the strain-stress relationship (see Fig. 6), the elastic modulus of the test sample can be estimated from the slope. To assure consistent contact between the pressing stamp and the tissue samples at the onset of deformations, measurement points were considered invalid if their associated force was less than ~10% of the maximal pressing force, which corresponds to ~10% of the strain range. Because of the uneven surface of the tissue samples, typical soft-tisue stress-strain relationships did not apply in this range. Those points with the natural strain greater than 30% were also discarded from elastic modulus estimation due to high deformability of the tissue samples.

### Histology

Sections of proximal and distal colon tissue (1 cm × 1 cm), adjacent to the matched sections that were used for the mechanical measurements, were collected for histology. Samples for histology were fixed in buffered formalin for <24 h, and embedded in paraffin. Five micron sections were made for mounting on slides, and Masson's trichrome staining were performed by the University of Michigan Cancer Center Histology and Immunoperoxidase Lab. Digital photomicrographs of proximal and distal colon sections were captured using an Olympus BX51 microscope at the University of Michigan Microscopy and Image Analysis Laboratory.

### Statistical analysis

The normal proximal bowel and abnormal distal bowel strains and Young's moduli in the TNBS-treated rats were each compared using a paired two-tailed *t*-test. A difference of the means with $p < 0.05$ was taken to be significant. To compare the strain estimates with the Young's modulus measurements, the strain estimates were correlated with the corresponding Young's modulus estimates in both the normal PBS rats and the abnormal TNBS rats. Because the proximal and distal segments were separated by at least 4 cm (7 cm – the distance from the anus to the most proximal sigmoid segment that was assess with strain imaging), we assumed that these measurements were independent for this analysis. Then to see if the strain and Young's modulus estimates were significantly correlated, we calculated the correlation coefficient between the two groups of measurements and compared the correlation coefficient with a null hypothesis of zero correlation using a two-tailed *t*-test.

## RESULTS

The major aim of this study is to demonstrate the feasibility of UEI to differentiate the mechanical property between control and TNBS-treated rats. To demonstrate the feasibility

of UEI to differentiate the mechanical property between TNBS-treated and untreated rats, we combined the respective PBS control animals ($n = 5$) and TNBS-treated animals ($n = 6$) from study 1 and study 2 for analysis. Although the two studies are different in duration and final dosage, both produced a fibrotic phenotype as characterized by gross pathology, histology and gene expression (data not shown). Therefore, the TNBS animals in both studies can be considered comparable in terms of fibrotic disease. To account for variable deformation force across different rats and different scan regions, strain images were normalized as described above.

The top panel in Fig. 4 depicts the representative normalized strain images along with the corresponding B-scans. The colon wall is approximately outlined by a dotted-lined ellipse in each image. The strain along the wall (red circles) clearly differentiates (c) abnormal area (distal) in a TNBS-treated rat (TNBS3 from study 2 in Table 1, Avg strain = $-0.3 \pm 0.1$, bright = hard) from (a) normal area (proximal) in the TNBS-treated rat (TNBS2 from study 1 in Table 1, Avg strain = $-2.5 \pm 0.2$, dark = soft) and (b) normal area (distal) in the PBS control rat (PBS1 from study 1 in Table 1, Avg strain= $-2.3 \pm 0.5$, dark = soft). The average of the strain for each scan was taken along the wall. Note there are some artifacts corresponding low correlated regions such as lumen contents (hyperechogenic material inside the circle) which are easily pushed out of the imaging cross section.

In the upper bottom panel of Fig. 4, corresponding gross dissection of the colon from (d, f) TNBS-treated and (e) PBS-treated rats are depicted. Excised colons are oriented from cecum (left) to rectum (right). The proximal colon (left) from all three animals is unaffected as indicated by a thin, translucent appearance in the top pictures. In contrast, the distal colon of TNBS-treated animals (d, f) exhibits a grossly fibrotic appearance, characterized by a shortened length (~3 cm shorter than the PBS control), marked thickening and apparent stiffness. The corresponding Trichrome staining for collagen in (d) unaffected proximal colon from a TNBS-treated animal compared with distal colon from (e) PBS control animal and (f) TNBS-treated animal are presented in the lower bottom panel. The locations of the histology staining are marked with black dots in the upper column of the right panel. Collagen (blue staining) is confined to a thin margin in the submucosal layer in the proximal colon of the TNBS-treated rat (d) and PBS control (e). In contrast, (f) the TNBS treated rat distal colon exhibits expansion of the smooth muscle layer with marked infiltration of collagen (blue staining).

A normal portion (proximal) and diseased portion (distal) of the colon from the TNBS-treated rats were also compared in Fig. 5. Normalized strain map (left panel) differentiates the diseased loop (red circle, distal, Avg strain = $-0.3 \pm 0.1$, bright = hard) from the normal loop (blue circle, proximal, Avg strain = $-3.4 \pm 0.1$, dark = soft) in a TNBS-treated rat (TNBS2 from study 2 in Table 1). Gross dissection of the colon is depicted in the upper right panel. Ultrasound imaging sections are indicated in the proximal colon (A) and distal colon (B). The distal colon exhibits marked thickening and stiffness with a characteristic curling of the most distal end. Corresponding trichrome staining for collagen in the unaffected proximal colon and affected distal colon are illustrated in the lower right panel. Collagen (blue staining) is confined to a thin margin in the submucosal layer in the normal proximal colon (A). In contrast, the diseased distal colon exhibits expansion of the smooth muscle layer, with marked infiltration of collagen (B). These observations are consistent throughout all the tissue samples in the study group. Overall the strain measurements of the entire population of the rats in the study group match well with histology and direct mechanical measurements (Table 1). The average normalized strains at proximal (normal) over five PBS control rats and six TNBS-treated rats was estimated to be $-2.6 \pm 0.5$ and that at distal (normal) over five PBS control rats was estimated to be $-2.7 \pm 0.7$, whereas the average normalized strain at distal (diseased) over six TNBS-treated rats was $-0.5 \pm 0.2$.

The stress–strain measurements from the Micro-Elastometer are presented in Fig. 6. Based on the strain–stress relationship, the elastic modulus of the test sample can be estimated from the slope. Within the strain range described in methods, first order polynomial (linear) fit was applied to estimate the slope of stress–strain curve, representing secant modulus (Table 1). $R^2$ represents the coefficient of determination for the curve fitting of the stress–strain relationship. From Fig. 6, the average elastic modulus of diseased area (distal) in a TNBS-treated rat (TNBS3 from study 2 in Table 1, solid red) was estimated to be 11.4 kPa, whereas that of the normal area (proximal) in the TNBS-treated rat (TNBS2 from study1 in Table 1, dash-dot blue) was 2.2 kPa and that of normal area (distal) in a PBS control rat (PBS1 from study1 in Table 1, dashed blue) was 4.9 kPa. The normalized strains from UEI and reconstructed elastic moduli from direct mechanical measurements are summarized in Table 1. The mean strain differences between the normal proximal segments and the abnormal distal segments in the TNBS-treated rats was highly significant ($p < 0.0002$), and the Young's moduli differences between the normal proximal segments and abnormal distal segments in the TNBS-treated rats were also significant ($p < 0.05$). Finally, the correlation coefficient between the strains and corresponding Young's modulus estimates over all 11 rats was 0.67, which is highly significant ($p < 0.0005$).

## DISCUSSION AND SUMMARY

The *in-vivo* measurements of strain by UEI correlated quite well with both histology and direct *ex-vivo* mechanical measurements of elastic modulus (Table 1). The elastic modulus is in the same order of magnitude as the elastic modulus of the soft tissue such as liver estimated by direct mechanical measurements (Yeh et al. 2002), MRI (Rouvière et al. 2006), and transient elastography (Gomez-Dominguez et al. 2006; Foucher 2006). The control and fibrotic animals were well differentiated by UEI. In a few cases, some artifacts such as ultrasound shadowing and unexpectedly high local strains were observed in ultrasound imaging because of the boundary conditions with surrounding tissues and lumen contents. These regions were not considered when taking the average strains based on their low correlation coefficients. We also found some difficulties with holding some loops of bowel stationary in the ultrasound imaging cross section because of a significant translational motion, especially for the proximal scans. Translational motion was minimized by applying mild restrictions by hand on both sides of the abdomen. The internal strain developed in the small cross section of the colon compared with the entire body will not be affected by this large scale translational motion restriction. Translation was not an issue for the distal sigmoid colon because of the sigmoid mesocolon, which tightly attaches the sigmoid to the posterior abdominal wall. This prevents lateral translation of this portion of bowel.

Histology by trichrome staining for collagen showed that collagen (blue staining) is confined to a thin margin in the submucosal layer in the normal proximal and distal colon while the diseased distal colon exhibits a substantial expansion of the smooth muscle layer with marked infiltration of collagen, disrupting the architecture of muscularis propria and submucosal layers with few inflammatory cells present, indicating a fibrotic as opposed to an inflammatory response. These observations are consistent throughout all the tissue samples in the study group.

The direct mechanical measurements also support the stiffness changes evidenced by UEI. The elastic modulus reconstructed from the stress-strain curve generated by MicroElastometer remained high for the diseased tissues compared with the normal tissues. The average elastic modulus proximally (normal) over five PBS control rats and six TNBS-treated rats was estimated to be 4.0 ± 1.5 kPa and that distally (normal) over five PBS control rats was estimated to be 5.5 ± 1.6 kPa, whereas the average elastic modulus distally (diseased) over six TNBS treated rats was 24.4 ± 18.7 kPa. Although caution was taken to

assure consistent contact between the pressing stamp and the tissue samples at the onset of deformations by considering the measurement points invalid if their associated force was <10% of the maximal pressing force and discarding those points with the natural strains >30% from elastic modulus estimation because of high deformability of the tissue samples, relatively high variations in elastic modulus estimates were observed. This was especially true for the elastic modulus estimates in the distal colon of TNBS-treated rats from the second study group, which varied considerably. This variation may be a result of unequal TNBS treatment effects with nonuniform fibrosis development producing inhomogeneous stiffness in the colon wall. Inhomogeneous stiffness also caused some sample to curl, making it difficult for these samples to lie flat on the Elastometer balance. When these curled samples were flattened, it may have caused an additional preload that would alter the stiffness of the tissue sample, introducing a large variance between the samples. However, even given this, the strains and the Young's modulus estimates were highly significantly correlated ($p < 0.0005$).

It is also notable that the elastic property of TNBS-treated, fibrotic tissue is very nonlinear compared with the normal tissues from the TNBS-treated rat and PBS control rat (Fig. 6). This observation also strongly suggests that ultrasound elasticity imaging can differentiate early stage inflammation (edema) from chronic fibrosis. Edema responds linearly to applied pressure, which generates a large strain until it completely pushes fluid out of the tissue (Bert et al. 1997; Parker et al. 1979). To the extent that the edema is interstitial fluid, this fluid does not act as an elastic medium. The fluid is displaced away from the site of deformation. Because the fluid in incompressible, the amount of fluid forced out of the slice corresponds to the fraction of the volume occupied by the interstitial fluid. Any nonlinearity will be a result of that fraction composed of tissue with elastic properties. Hence, if the volume mostly fluid, the response will tend toward being linear. If the deformed volume is mostly tissue/fibrosis, the response will tend toward being nonlinear. Investigations on nonlinearity will add important parameters to fully assess and monitor the mechanical property change in the process of Crohn's disease development.

Preliminary results in this study indicate the feasibility of translating UEI into a clinical diagnostic and monitoring tool for Crohn's disease. There may be several challenges. First, we may have difficulty in finding narrowed bowel segments in human subjects using ultrasound. However, we realistically do not think this will be an issue. Physicians routinely use diagnostic CT scans to locate the diseased loops of bowel. Once the diseased loops are identified, it is a simple matter to use ultrasound to evaluate these loops for fibrosis. This is very similar to the ability of ultrasound to evaluate appendicitis and other inflammatory diseases of the cecum where any overlying normal bowel loops can be preloaded to remove the luminal contents or gas (Puylaert 1986, Puylaert 2001). Gas and lumen contents are free to move out of the imaging sections, and hence represent highly deformable soft structures in elasticity imaging (Puylaert 1986, Puylaert 2001). They will absorb essentially all of the strain in a deformation until they are removed. Thus any strains in abnormal loops will not be affected by this preloading. Clinically, it could be possible that the physicians would not find the affected loops in a morbidly obese patient, but that seems very unlikely given that most Crohn's patients, particularly those with strictures requiring surgery, are generally underweight because of malnutrition.

Secondly, UEI may prove to have difficulties with translation of stress, as the small intestine moves freely in the peritoneum. To overcome this issue, the physicians can always manipulate the deformation so that the compression can be directed toward a solid object such as bone or spine. Finally, it may prove to be difficult to compress narrowed segments of small intestine against the spine or pelvis. Although deformations against bone are preferable, the physicians can also deform against other soft tissues once the bowel has been

preloaded to remove gas. In some sense, this is analogous to what is now done with deformations made in strain imaging of the prostate where the prostate is deformed from its posterior surface against anterior soft tissues (Miyanaga et al. 2006; Cochlin et al. 2002; Lorenz et al. 2000).

In conclusion, preliminary results with animal model demonstrate that UEI can detect the stiffness change as a result of fibrosis development, with reasonably high sensitivity and reproducibility. For more significant statistics, a large scale animal study is planned, including antifibrotic treatment. UEI will advance the ability to identify and measure intestinal fibrosis, which will allow more rapid and directed therapy for patients with intestinal fibrosis. The development of an accurate noninvasive method to measure intestinal fibrosis would allow clinical development and evaluation of candidate antifibrotic therapies that may attenuate or reverse intestinal fibrosis.

## Acknowledgments

This work was supported in part by NIH grants HL-67647, HL-68658, HL-082640 and CA-109440. We Philips Ultrasound, Bothell, WA, USA, for their system support.

## REFERENCES

Baldewsing RA, Schaar JA, Mastik F, van der Steen AFW. Local elasticity imaging of vulnerable atherosclerotic coronary plaques. Advances in Cardiol. 2007; 44:35–61.

Bert JL, Reed RK. Pressure-volume relationship for rat dermis: Compression studies. Acta Physiol Scand. 1997; 160:89–94. [PubMed: 9179316]

Bertrand, M.; Meunier, J.; Doucet, M.; Ferland, G. Ultrasonic biomechanical strain gauge based on speckle tracking; Proceedings of the 1989 IEEE Ultrasonics Symposium 0090–5607–89; 1989. p. 859-864.

Bilgen M, Insana MF. Deformation models and correlation analysis in elastography. J Acoust Soc Am. 1996; 99:3212–3224. [PubMed: 8642127]

Browse, NL.; Burnand, KG.; Irvine, AT.; Wilson, NM. CHAPTER TITLE. In: Browse, NL.; Burnand, KG.; Irvine, AT., et al., editors. Disease of the Veins. London: Arnold; 1999. p. 249-289.

Booi RC, O'Donnell M, Knoth MM, Xie H, Hall AL, Rubin JM, Carson PL. 3D breast elastography with a combined ultrasound/tomography system. IEEE Ultrasonics Symp. 2006:2056–2059.

Booi RC, Carson PL, Erkamp RQ, Xie H, Kapur A, LeCarpentier GL, Roubidoux MA, Fowlkes JB, O.Donnell M. Applying in vitro elasticity imaging results to optimize in vivo breast lesion characterization using a combined 3D ultrasound/digital x-ray system. IEEE Ultrasonics Symp. 2005:727–730.

Castera L, Vergniol J, Foucher J, et al. Prospective comparison of transient elastography, Fibrotest, APRI, and liver biopsy for the assessment of fibrosis in chronic hepatitis C. Gastroenterology. 2005; 128:343–350. [PubMed: 15685546]

Choi, CD.; Shapo, BM.; Lubinski, MA.; Crowe, JR.; Skovoroda, AR.; Emelianov, SY.; O'Donnell, M. Elasticity imaging to monitor plaque rupture; Presented at the 1999 Ultrasonic Imaging and Tissue Characterization Conference. Ultrasonic Imaging; 1999. p. 72-73.

Cochlin DL, Ganatra RH, Griffiths DF. Elastography in the detection of prostatic cancer. Clin Radiol. 2002; 57(11):1014–1020. [PubMed: 12409113]

De Franchis R, Dell'Era A. Non-invasive diagnosis of cirrhosis and the natural history of its complications. Best Pract Res Clin Gastroenterol. 2007; 21(1):3–18. Review. [PubMed: 17223493]

de Korte, CL.; Woutman, HA.; van der Steen, AFW.; Cespedes, EI.; Pasterkamp, G. IVUS elastography: A potential identifier of vulnerable atherosclerotic plaque; Proceedings of the 1998 IEEE Ultrasonics Symposium 98CH36102; 1998. p. 1729-1732.

Di Sabatino A, Armellini E, Corazza GR. Doppler sonography in the diagnosis of inflammatory bowel disease. Digest Dis. 2004; 22:63–66.

Downing LJ, Strieter RM, Kadell AM, Wilke CA, Brown SL, Wrobleski SK, Burdick MD, Hulin MS, Fowlkes JB, Greenfield LJ, Wakefield TW. Neutrophils are the initial cell type identified in deep venous thrombosis induced vein wall inflammation. ASAIO J. 1996; 42:M677–M682. [PubMed: 8944966]

Emelianov SY, Eberle MJ, Stephens DN, Litzza JL, Shapo BM, Crowe JR, Choi CD, Chen JJ, Ziegenbein RC, Wu CC, Bleam D, Skovoroda AR, O'Donnell M. Reconstructive ultrasound elasticity imaging of coronary artery using catheter arrays. Annals of Biomedical Engineering. 1998a; vol. 26 Suppl 1:S-55.

Emelianov, SY.; Rubin, JM.; Lubinski, MA.; Skovoroda, AR.; O'Donnell, M. Elasticity imaging of the liver: Is hemangioma hard or soft?"; Proceedings of the 1998 IEEE Ultrasonics Symposium; 1998b. p. 1749-1752.

Feagan BG, Vreeland MG, Larson LR, Bala MV. Annual cost of care for Crohn's disease: A payor perspective. Am J Gastroenterol. 2000; 95:1955–1960. [PubMed: 10950042]

Foucher J, Chanteloup E, Vergniol J, Castera L, Le Bail B, Adhoute X, Bertet J, Couzigou P, de Ledinghen V. Diagnosis of cirrhosis by transient elastography (FibroScan): A prospective study. Gut. 2006; 55:403–408. [PubMed: 16020491]

Fraquelli M, Colli A, Casazza G, Paggi S, Colucci A, Massironi S, Duca P, Conte D. Role of US in detection of Crohn disease: Meta-analysis. Radiology. 2005; 236:95–101. [PubMed: 15987966]

Froehlich F, Juillerat P, Mottet C, Felley C, Vader JP, Burnand B, Gonvers JJ, Michetti P. Obstructive fibrostenotic Crohn's disease. Digestion. 2005; 71:29–30. [PubMed: 15711046]

Gao L, Parker KJ, Lerner RM, Levinson SF. Imaging of the elastic properties of tissue—A review. Ultrasound Med Biol. 1996; 22:959–977. [PubMed: 9004420]

Garra BS, Céspedes EI, Ophir J, Spratt RS, Zuurbier RA, Magnant CM, Pennanen MF. Elastography of breast lesions: Initial clinical results. Radiology. 1997; 202:79–86. [PubMed: 8988195]

Geiman BJ, Bohs LN, Anderson ME, Breit SM, Trahey GE. A novel interpolation strategy for estimating subsample speckle motion. Phys Med Biol. 2000; 45:1541–1552. [PubMed: 10870709]

Gomez-Dominguez E, Mendoza J, Rubio S, Moreno-Monteagudo JA, Garcia-Buey L, Moreno-Otero R. Transient elastography: A valid alternative to biopsy in patients with chronic liver disease. Alimentary Pharmacol Ther. 2006; 24:513–518.

Hall, TJ.; Zhu, Y.; Spalding, CS.; Cook, LT. In vivo results real-time free hand elasticity imaging; In Proc IEEE Ultrason Symp; 2001. p. 1653-1657.

Hall TJ, Zhu Y, Spalding CS. In vivo real-time freehand palpation imaging. Ultrasound Med Biol. 2003; 29:427–436. [PubMed: 12706194]

Insana MF, Hall TJ. 2-D Companding for noise reduction in strain imaging. IEEE Trans UFFC. 1998; 45:179–191.

Kim K, Weitzel WF, Rubin JM, Xie H, Chen X, O‖Donnell M. Vascular intramural strain imaging using vessel pressure equalization. Ultrasound Med Biol. 2004; 30(6):761–771. [PubMed: 15219956]

Konofagou EE, Ophir J. A new method for estimation and imaging of lateral strains and Poisson's ratios in tissues. Ultrasound Med Biol. 1998; 24:1183–1199. [PubMed: 9833588]

Kratzer W, Schmidt SA, Mittrach C, Mittrach C, Haenle MM, Mason RA, Von Tirpitz C, Pauls S. Contrast-enhanced wideband harmonic imaging ultrasound (SonoVue): A new technique for quantifying bowel wall vascularity in Crohn's disease. Scan J Gastro. 2005; 40:985–991.

Krouskop TA, Wheeler TM, Kallel F, Garra BS, Hall T. Elastic modulus of breast and prostate tissues under compression. Ultrasonic Imaging. 1998; 20:260–274. [PubMed: 10197347]

Lawrance IC, Wu F, Leite AZ, Willis J, West GA, Fiocchi C, Chakravarti S. A murine model of chronic inflammation-induced intestinal fibrosis down-regulated by antisense NF-kappa B. Gastroenterology. 2003; 125(6):1750–1761. [PubMed: 14724828]

Lerner RM, Parker KJ, Holen J, Gramiak R, Waag RC. Sono-elasticity: Medical elasticity images derived from ultrasound signals in mechanically vibrated targets. Acoust Imaging. 1988; 16:317–327.

Lerner RM, Huang SR, Parker KJ. Sonoelasticity images derived from ultrasound signals in mechanically vibrated tissues. Ultrasound Med Biol. 1990; 16:231–239. [PubMed: 1694603]

Loftus EV Jr, Schoenfeld P, Sandborn WJ. The epidemiology and natural history of Crohn's disease in population-based patient cohorts from North America: A systematic review. Aliment Pharmacol Ther. 2002; 16:51–60. [PubMed: 11856078]

Lorenz A, Ermert H, Sommerfeld HJ, Garcia-Schurmann M, Senge T, Philippou S. Ultrasound elastography of the prostate. A new technique for tumor detection. Ultraschall in der Medizin. 2000; 21(1):8–15. [PubMed: 10746278]

Lorenz A, Sommerfield HJ, Garcia-Schurmann MG, Philippou S, Senge T, Ermert H. A new system for the acquisition of ultrasonic multi-compression strain images of human prostate in vivo. IEEE Ultrason, Ferroelectr Freq Control. 1999; 46:1147–1154.

Louis E, Collard A, Oger AF, Degroote E, Aboul Nasr El Yafi FA, Belaiche J. Behaviour of Crohn's disease according to the Vienna classification: Changing pattern over the course of the disease. Gut. 2001; 49:777–782. [PubMed: 11709511]

Lubinski MA, Emelianov SY, Raghavan KR, Yagle AE, Skovoroda AR, O'Donnell M. Lateral displacement estimation using tissue incompressibility. IEEE Trans Ultrason, Ferroelectr Freq Control. 1996; 43(2):247–256.

Lubinski MA, Emelianov SY, O'Donnell M. Speckle tracking methods for ultra sonic elasticity imaging using short time correlation. IEEE Trans Ultrason Ferroelectr Freq Control. 1999; 46:82–96. [PubMed: 18238401]

Lyshchik A, Higashi T, Asato R, Tanaka S, Ito J, Hiraoka M, Insana MF, Brill AB, Saga T, Togashi K. Cervical lymph node metastases: Diagnosis at sonoelastography—Initial experience. Radiology. 2007; 243:258–267. [PubMed: 17293571]

Lyshchik A, Higashi T, Asato R, Tanaka S, Ito J, Mai JJ, Pellot-Barakat C, Insana MF, Brill AB, Saga T, Hiraoka M, Togashi K. Thyroid gland tumor diagnosis at US elastography. Radiology. 2005:202–211. [PubMed: 16118150]

Maconi G, Di Sabatino A, Ardizzone S, Greco S, Colombo E, Russo A, Cassinotti A, Casini V, Corraza GR, Porro GB. Prevalence and clinical significance of sonographic detection of enlarged regional lymph nodes in Crohn's disease. Scan J Gastroenterol. 2005; 40:1328–1333.

Maconi G, Radice E, Greco S, Bianchi Porro G. Bowel ultrasound in Crohn's disease. Best Pract Res Clin Gastroenterol. 2006; 20:93–112. [PubMed: 16473803]

Mayer D, Reinshagen M, Mason RA, Muche R, von Tirpitz C, Eckelt D, Adler G, Beckh K, Kratzer W. Sonographic measurement of thickened bowel wall segments as a quantitative parameter for activity in inflammatory bowel disease. Zeitschrift für Gastroenterologie. 2000; 38:295–300.

Miyanaga N, Akaza H, Yamakawa M, Oikawa T, Sekido N, Hinotsu S, Kawai K, Shimazui T, Shiina T. Tissue elasticity imaging for diagnosis of prostate cancer: A preliminary report International. J Urol. 2006; 13:1514–1518.

Morris GP, Beck PL, Herridge MS, Depew WT, Szewczuk MR, Wallace JL. Hapten-induced model of chronic inflammation and ulceration in the rat colon. Gastroenterology. 1989; 96(3):795–803. PMID:2914642. [PubMed: 2914642]

O'Donnell, M.; Skovoroda, AR.; Shapo, BM. Measurement of vessel wall motion using Fourier based speckle tracking algorithms; Proceedings of the 1991 IEEE Ultrasonics Symposium, IEEE 91CH3079-1; 1991. p. 1101-1104.

Ophir J, Céspedes I, Ponnekanti H, Yazdi Y, Li X. Elastography: A quantitative method for imaging the elasticity of biological tissues. Ultrasonic Imaging. 1991; 13:111–134. [PubMed: 1858217]

Ophir J, Céspedes I, Garra B, Ponnekanti H, Huang Y, Maklad N. Elastography: Ultrasonic imaging of tissue strain and elastic modulusin vivo. Eur J Ultrasound. 1996; 3:49–70.

Parente F, Greco S, Molteni M, Anderloni A, Maconi G, Porro GB. Modern imaging of Crohn's disease using bowel ultrasound. Inflamm Bowel Dis. 2004; 10:452–461. [PubMed: 15475759]

Parente F, Greco S, Molteni M, Anderloni A, Bianchi Porro G. Imaging inflammatory bowel disease using bowel ultrasound. Euro J Gastroenterol Hepatol. 2005; 17:283–291.

Parker JC, Falgout KJ, Parker RE, Granger DN, Taylor AE. The effect of fluid volume loading on exclusion of interstitial albumin and lymph flow in the dog lung. Circ Res. 1979; 45:440–450. [PubMed: 476867]

Perk G, Tunick PA, Kronzon I. Non-Doppler two-dimensional strain imaging by echocardiography—From technical considerations to clinical applications. J Am Soc Echocardiogr. 2007; 20:234–243. [PubMed: 17336748]

Puylaert JB. Acute appendicitis: US evaluation using graded compression. Radiology. 1986; 158:355–360. [PubMed: 2934762]

Puylaert JB. Ultrasound of acute GI tract conditions. Euro Radiol. 2001; 11:1867–1877.

Rekhter M, Kindt E, Hallak H, Choi CD, O'Donnell M, Rosebury W, Hicks G, Brammer D, Ryan M. Even hardened arteries have their soft spots. Presented at the 1999 Meeting of the North American Vascular Biology Organization, FASEB J. 1999; 13(4):A206.

Robotti D, Cammarota T, Debani P, Sarno A, Astegiano M. Activity of Crohn disease: Value of color-power-Doppler and contrast-enhanced ultrasonography. Abdom Imaging. 2004; 29:648–652. [PubMed: 15162232]

Rouvière O, Yin M, Dresner MA, Rossman PJ, Burgart LJ, Fidler JL, Ehman RL. MR elastography of the liver: Preliminary results. Radiology. 2006; 240:440–448. [PubMed: 16864671]

Rubin JM, Aglyamov SR, Wakefield TW, O'Donnell M, Emelianov SY. Clinical application of sonographic elasticity imaging for aging of deep venous thrombosis: preliminary findings. J Ultrasound Med. 2003; 22:443–448. [PubMed: 12751855]

Rubin JM, Xie H, Kim K, Weitzel WF, Emelianov SY, Aglyamov SR, Wakefield TW, Urquhart AG, O'Donnell M. Sonographic elasticity imaging of acute and chronic DVT in humans. J Ultrasound Med. 2006; 25(9):1179–1186. [PubMed: 16929019]

Ryan, LK.; Lockwood, GR.; Starkoski, BG.; Holdsworth, DW.; Rickey, DW.; Drangova, M.; Fenster, A.; Foster, FS. A high frequency intravascular imaging system for investigation of vessel wall properties; Proceedings of the 1992 IEEE Ultrasonics Symposium 92CH3118–7; 1992. p. 1101-1105.

Sallomi DF. The use of contrast-enhanced power Doppler ultrasound in the diagnosis and follow-up of inflammatory abdominal masses associated with Crohn's disease. Eur J Gastroentol Hepatol. 2003; 15:253–259.

Sands BE, Arsenault JE, Rosen MJ, Alsahli M, Bailen L, Banks P, Bensen S, Bousvaros A, Cave D, Cooley JS, Cooper HL, Edwards ST, Farrell RJ, Griffin MJ, Hay DW, John A, Lidofsky S, Olans LB, Peppercorn MA, Rothstein RI, Roy MA, Saletta MJ, Shah SA, Warner AS, Wolf JL, Vecchio J, Winter HS, Zawacki JK. Risk of early surgery for Crohn's disease: Implications for early treatment strategies. Am J Gastroenterol. 2003; 98:2712–2718. [PubMed: 14687822]

Sarvazyan, AP.; Skovoroda, AR. The new approaches in ultrasonic visualization of cancers and their qualitative mechanical characterization for the differential diagnostics. Abstract of the All-Union Conference; The Actual Problems of the Cancer Ultrasonic Diagnostics; Moscow. 1990.

Shapo, BM.; Crowe, JR.; Skovoroda, ARAR.; Eberle, MJ.; Cohn, NA.; O'Donnell, M. Ultrasonic displacement and strain imaging of coronary arteries with a catheter array; Proceedings of the 1995 IEEE Ultrasonics Symposium; 1995. p. 1511-1514.95CH35844

Silverstein MD, Loftus EV, Sandborn WJ, Tremaine WJ, Feagan BG, Nietert PJ, Harmsen WS, Zinsmeister AR. Clinical course and costs of care for Crohn's disease: Markov model analysis of a population-based cohort. Gastroenterology. 1999; 117:49–57. [PubMed: 10381909]

Skovoroda AR, Emelianov SY, Lubinski MA, Sarvazyan AP, O'Donnell M. Theoretical analysis and verification of ultra sound displacement and strain imaging. IEEE Trans UFFC. 1994; 41:302–313.

Tristam M, Barbosa DC, Cosgrove DO, Bamber JC, Hill CR. Application of Fourier analysis to clinical study of patterns of tissue motion. Ultrasound Med Biol. 1988; 14:695–707. [PubMed: 3062864]

van der Steen, AFW.; Cespedes, EI.; de Korte, CL.; Carlier, SG.; Li, W.; Mastik, F.; Lancee, CT.; Borsboom, J.; Lupotti, F.; Krams, R.; Serruys, PW.; Bom, N. Novel developments in intravascular imaging; Proceedings of the 1998 IEEE Ultrasonics Symposium (invited paper) 98CH36102; 1998. p. 1733-1742.

Weitzel WF, Kim K, Rubin JM, Wiggins RC, Xie H, Chen X, Emelianov SY, O'Donnell M. Feasibility of applying ultrasound strain imaging to detect renal transplant chronic allograft nephropathy. Kidney Int. 2004; 65(2):733–736. [PubMed: 14717949]

Weitzel WF, Kim K, Rubin JM, Xie H, Chen X, O'Donnell M. Renal advances in ultrasound elasticity imaging: Measuring the compliance of arteries and kidneys in end-stage renal disease. Blood Purif. 2005; 23:10–17. [PubMed: 15627731]

Xie H, Kim K, Aglyamov SR, Emelianov SY, O'Donnell M, Weitzel WF, Wrobleski SK, Myers DD, Wakefield TW, Rubin JM. Correspondence of ultrasound elasticity imaging to direct mechanical measurement in aging DVT in rats. Ultrasound Med Biol. 2005; 31(10):1351–1359. [PubMed: 16223638]

Xie H, Kim K, Aglyamov SR, Emelianov SY, Chen X, O'Donnell M, Weitzel WF, Wrobleski SK, Myers DD, Wakefield TW, Rubin JM. Staging deep venous thrombosis using ultrasound elasticity imaging: Animal model. Ultrasound Med Biol. 2004; 30(10):1385–1396. [PubMed: 15582239]

Yamakoshi Y, Sato J, Sato T. Ultrasonic imaging of internal vibration of soft tissue under forced vibration. IEEE Transactions on UFFC. 1990; 37:45–53.

Yeh W-C, Li P-C, Jeng Y-M, Hsu H-C, Kuo P-L, Li M-L, Yang P-M, Po HL. Young's modulus measurements of human liver and correlation with pathological findings. Ultrasound Med Biol. 2002; 28:467–474. [PubMed: 12049960]

Ziol M, Handra-Luca A, Kettaneh A, et al. Noninvasive assessment of liver fibrosis by measurement of stiffness in patients with chronic hepatitis C. Hepatology. 2005; 41:48–54. [PubMed: 15690481]

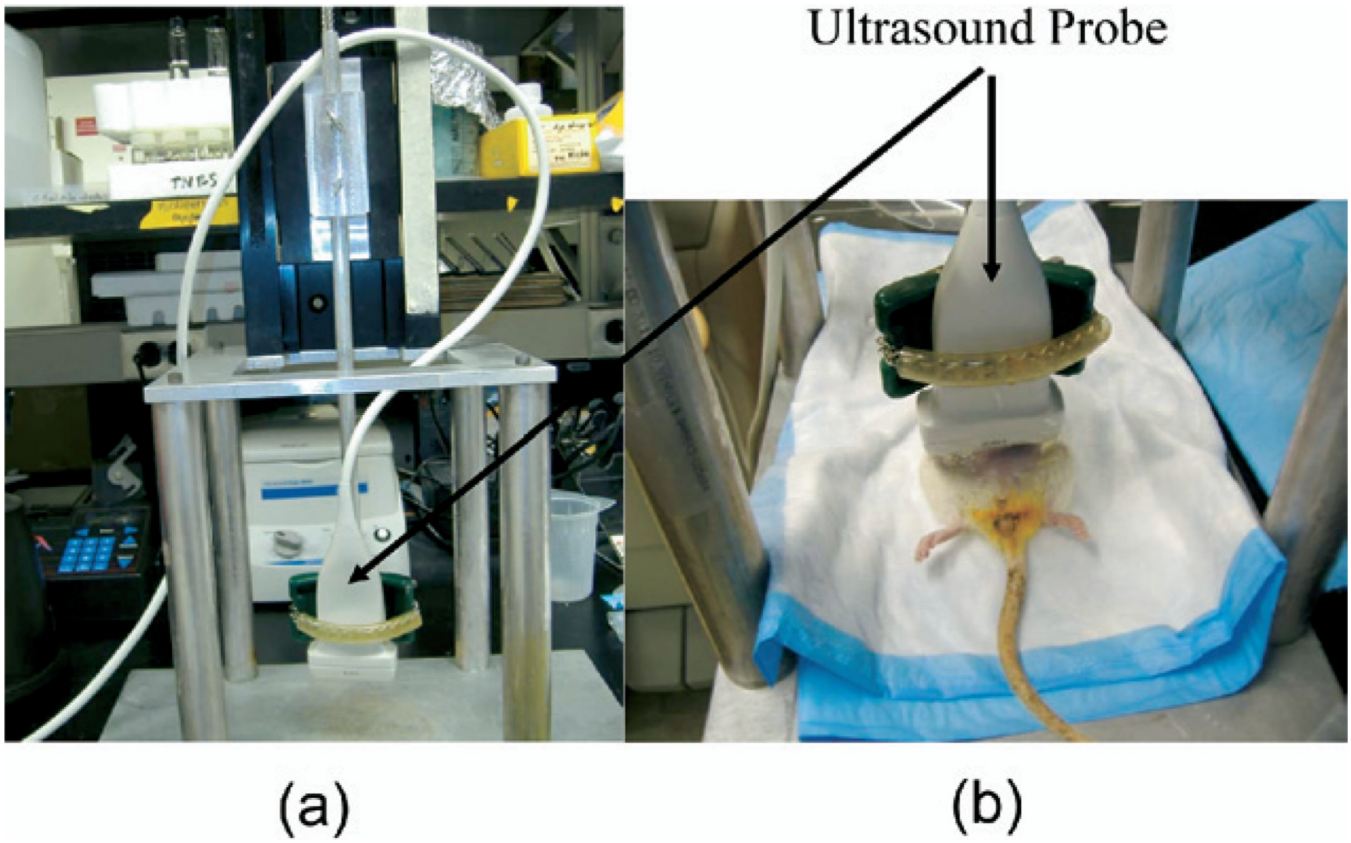


**Fig. 1.**
Deformation device. (a) The ultrasound transducer was fixed to a laboratory designed deformation device and (b) anesthetized rats were placed on a platform in a supine position with the abdomen exposed to the transducer.

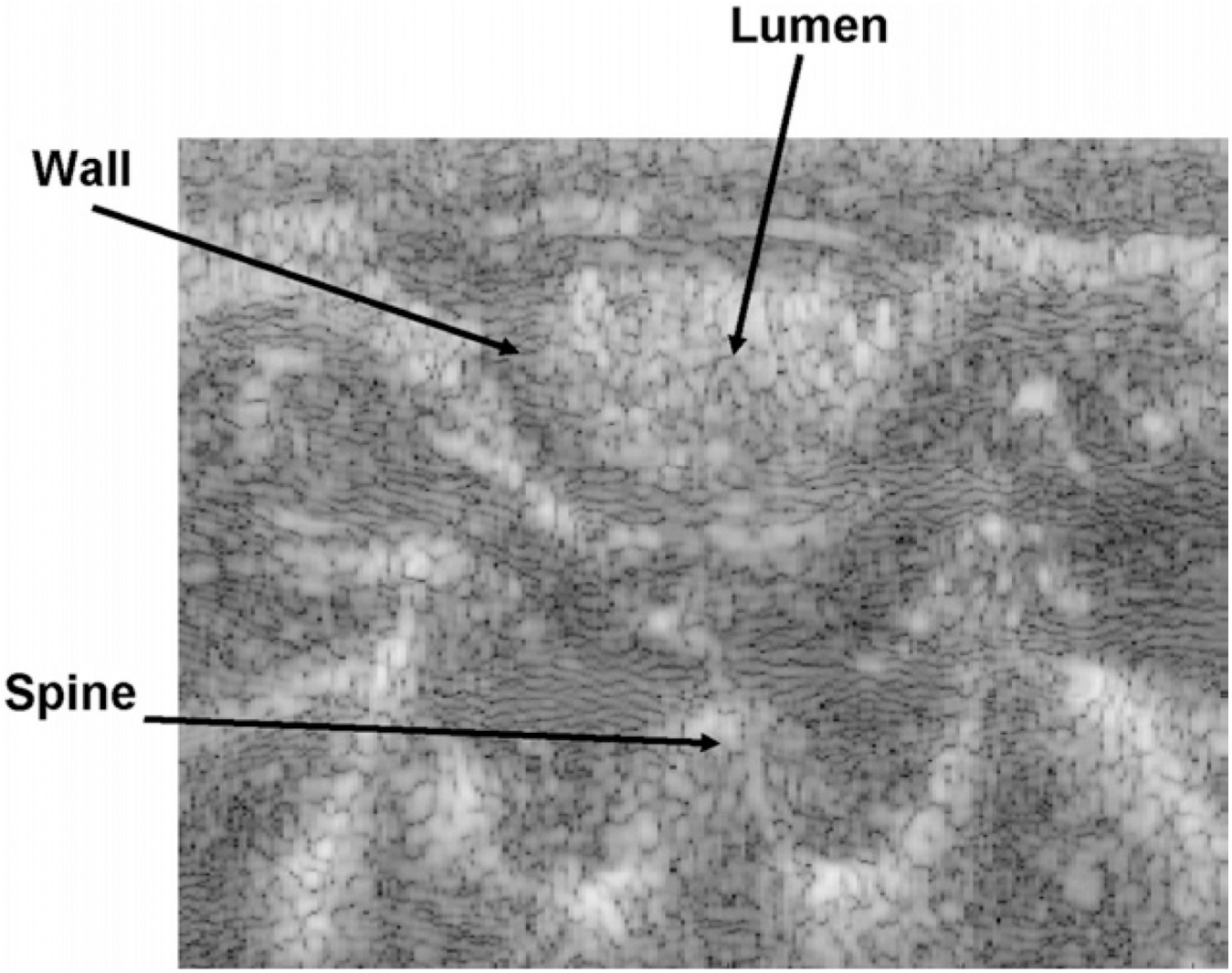


**Fig. 2.**
Typical ultrasound image view. Hypoechogenic circle around hyperechogenic bowel contents in the lumen represents the colon wall. The strain developed inside of the intestinal wall is normalized to the average strain estimated by the displacement of the spine relative to the surface of the transducer.

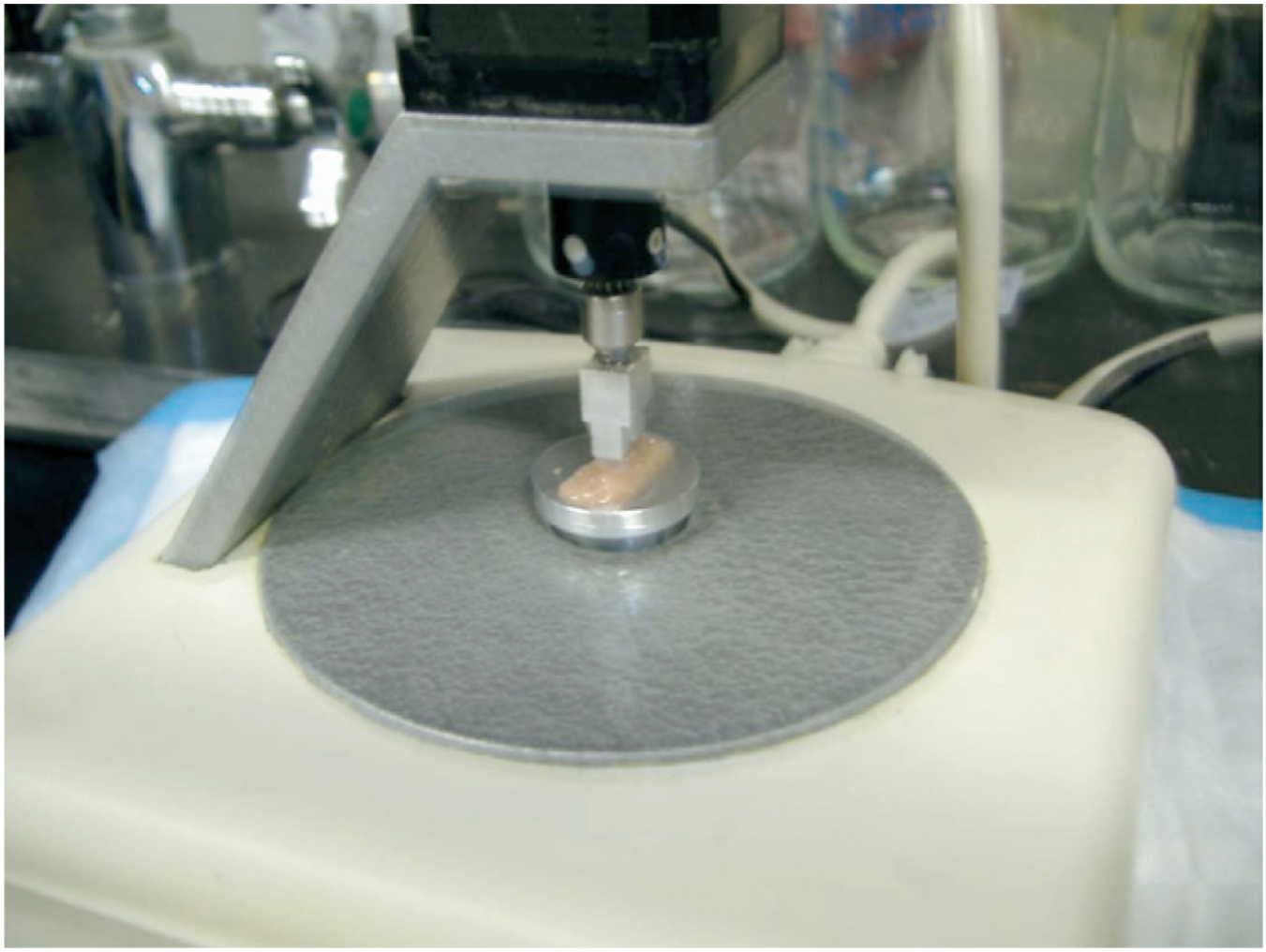

**Fig. 3.**
Direct mechanical measurement device (MicroElastometer). The MicroElastometer measures the displacement *vs.* force while a test sample on the object plate is subject to compression by a rectangular stamp of 8.88 mm by 3.98 mm.

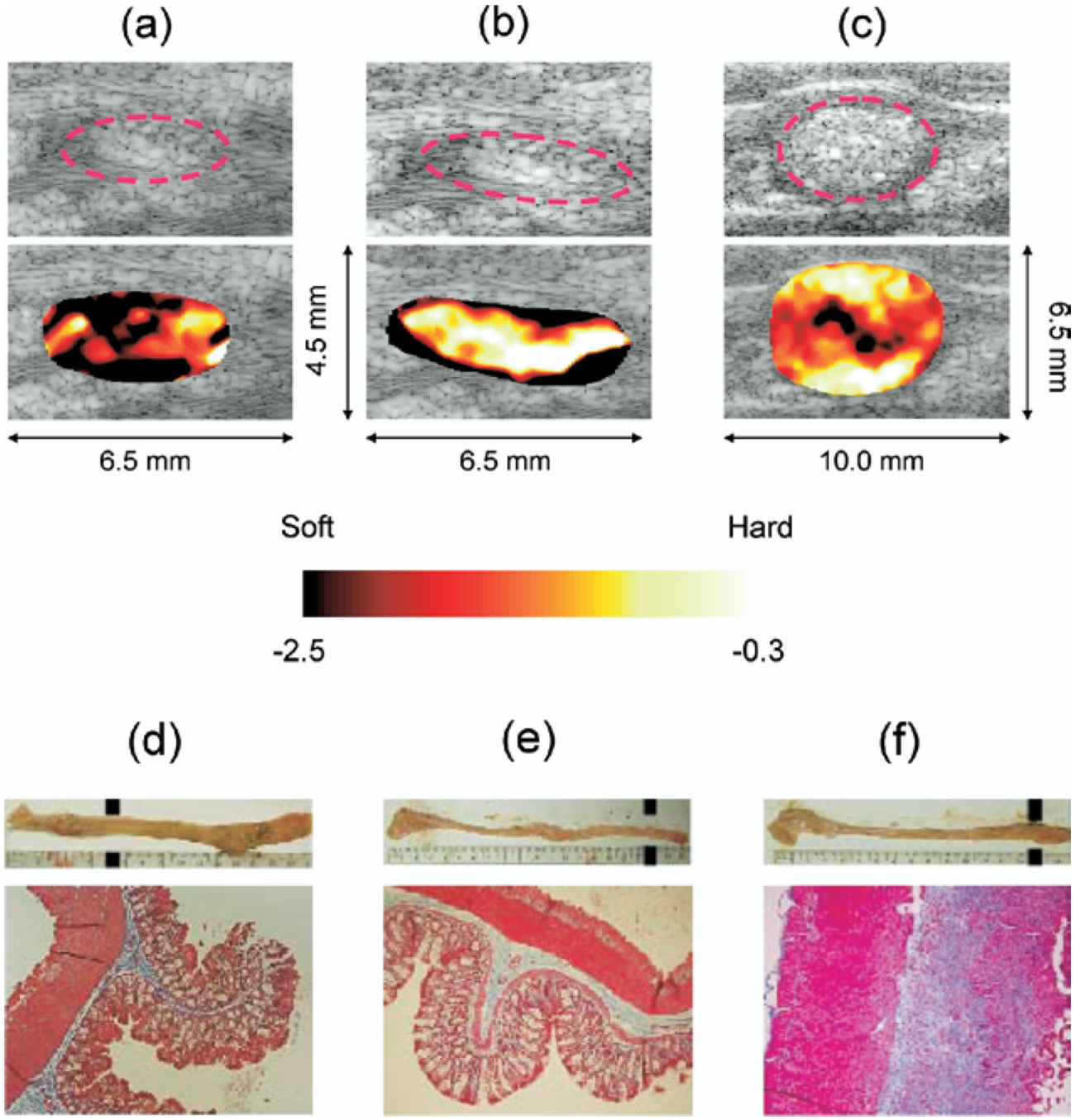


**Fig. 4.**

Normalized elasticity imaging and histology. Top Panel: (a) normal area in a TNBS-treated rat (Avg strain = −2.5 ± 0.2); (b) normal area in a PBS-controlled rat (Avg strain = −2.3 ± 0.5); and (c) diseased area in a TNBS-treated rat (Avg strain = 0.3 ± 0.1). Note the red dotted circles follow the hypoechogenic intestine walls. Upper bottom panel: Gross dissection of the colon from (d, f) TNBS-treated and (e) PBS-treated rats. Excised colons are oriented from cecum (left) to rectum (right). The proximal colon (left) from all three animals is unaffected as indicated by a thin, translucent appearance. In contrast, the distal colon of TNBS-treated animals (d, f) exhibits a grossly fibrotic appearance, characterized by a shortened length (~3 cm shorter than the PBS control), marked thickening, and stiffness with

a characteristic curling of the most distal end. Lower bottom panel corresponding trichrome staining for collagen in (d) unaffected proximal colon from a TNBS-treated animal compared with distal colon from (e) PBS control animal and (f) TNBS-treated animal. In the matched histologic sections, the unaffected sigmoid colon collagen (blue staining) is confined to a thin layer of the submucosa in both the TNBS-treated rat (d) and PBS control (e). In contrast, (f) the TNBS-treated rat distal colon exhibits substantial expansion of the smooth muscle layers and collagen infiltration (blue staining) of the submucosal and muscularis layers with few inflammatory cells present, indicating a fibrotic as opposed to an inflammatory response.

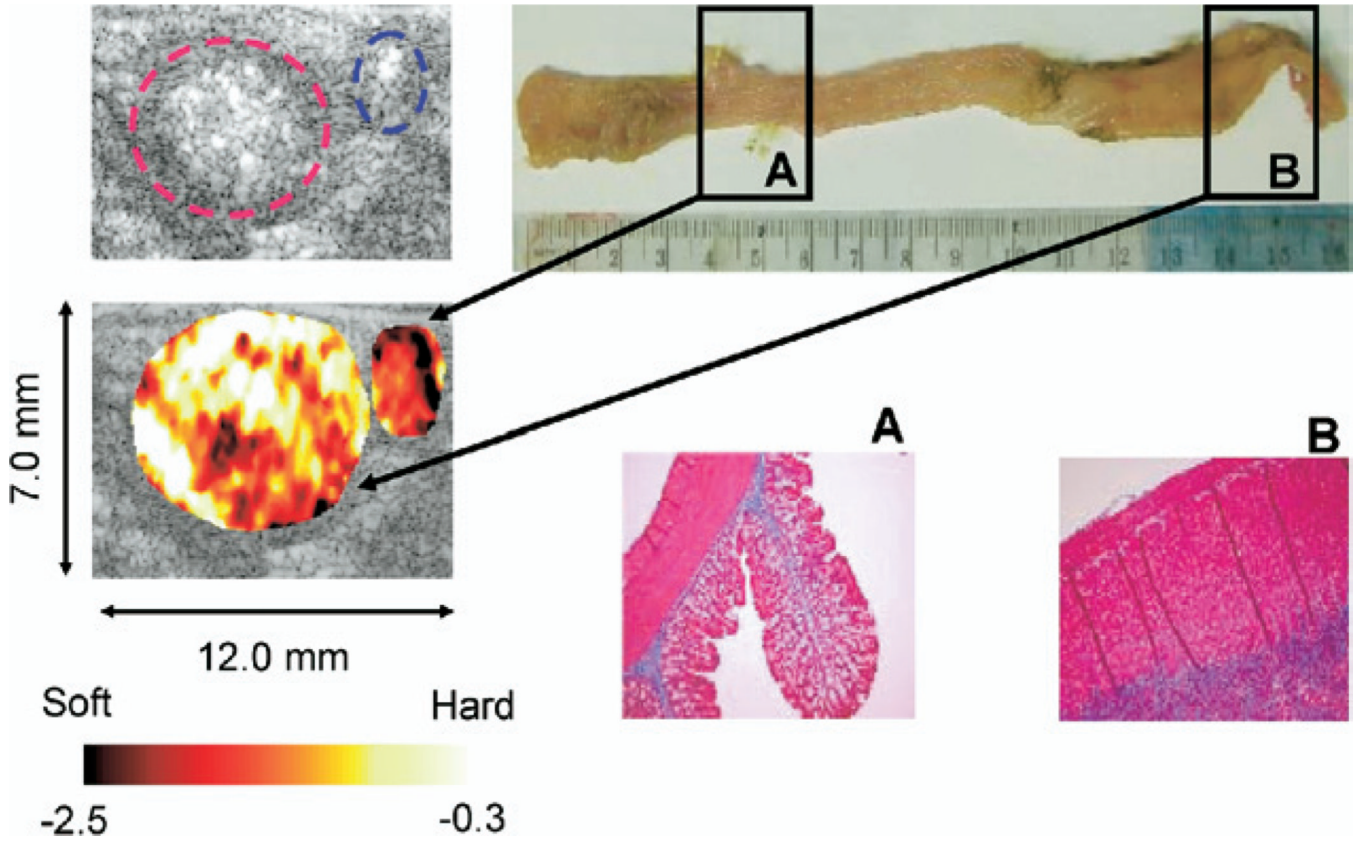


**Fig. 5.**

Normalized elasticity imaging (left panel) of a diseased loop (red circle) and normal loop (blue circle) in the same TNBS-treated rat. Upper right panel: Gross dissection of the colon. Ultrasound ROI are indicated in the proximal colon (A) and distal colon (B). The distal colon exhibits marked thickening and stiffness with a characteristic curling of the most distal end. Lower right panel: Histologic sections of representative areas of unaffected sigmoid (A) and affected distal colon (B) from the same animal. The elasticity images and the histologic sections were not precisely matched. Trichrome staining for collagen is shown in blue. Collagen (blue staining) is confined to a thin margin in the submucosal layer exhibits expansion of the smooth muscle layer with marked infiltration of collagen.

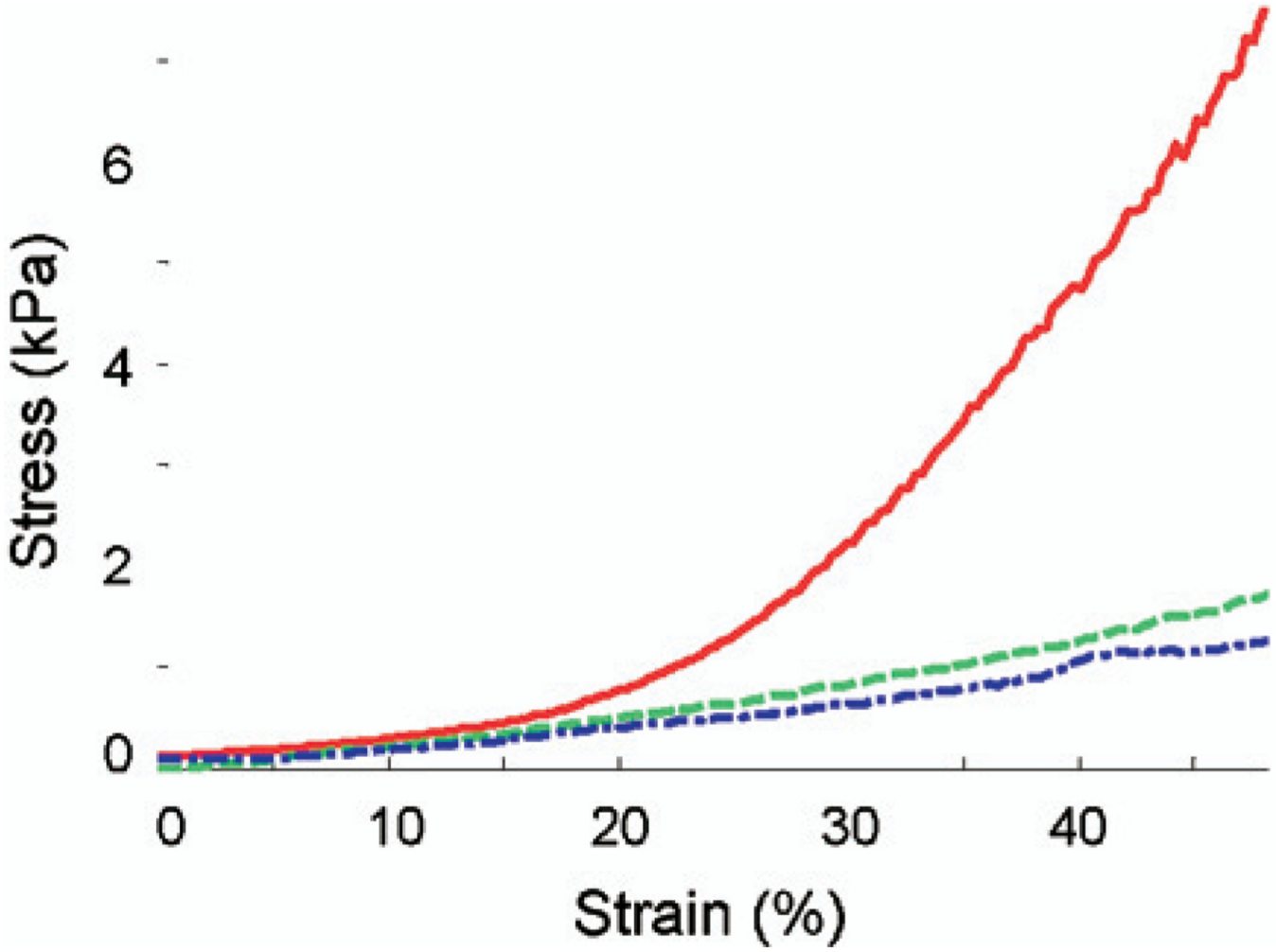


**Fig. 6.**

Direct mechanical measurement of the dissected tissues. The tissue samples are from the rats used for strain measurements presented in Fig. 3. Solid red: diseased area (distal) in a TNBS-treated rat (TNBS3 from study 2 in Table 1, 11.4 kPa); dash-dot blue: normal area (proximal) in the TNBS-treated rat (TNBS2 from study 1 in Table 1, 2.2 kPa); dashed green: normal area (distal) in a PBS control rat (PBS1 from study 1 in Table 1, 4.9 kPa). The elastic modulus was calculated by taking the slope of the linear fit of each curve within the strain range of 10% to 30%. Note that diseased tissue in TNBS-treated rat also demonstrates a high nonlinearity compared with a normal tissue from the TNBS-treated rat and PBS control rat.

**Table 1**

Elastic modulus reconstructed from stress-strain curve (figure 6) and normalized strains of the rats used in the study. $R^2$ represents the coefficient of determination for the curve fitting of the stress-strain relationship.

| Study Number | Subject Number | | E(kPa) | Correlation($R^2$) | Normalized Strain |
|---|---|---|---|---|---|
| | | Proximal | 4.6 | 0.9763 | −1.6 +/− 0.1 |
| | PBS1 | Distal | 4.9 | 0.9568 | −2.3 +/− 0.5 |
| | | Proximal | 4.8 | 0.9533 | −2.3 +/− 0.3 |
| | PBS2 | Distal | 5.3 | 0.8979 | −2.4 +/− 0.3 |
| | | Proximal | 5.3 | 0.9186 | −2.4 +/− 0.3 |
| | TNBS1 | Distal | 15.3 | 0.8968 | −0.6 +/− 0.1 |
| | | Proximal | 2.2 | 0.9956 | −2.5 +/− 0.2 |
| | TNBS2 | Distal | 11.7 | 0.9270 | −0.7 +/− 0.1 |
| | | Proximal | 4.6 | 0.9468 | −2.6 +/− 0.3 |
| Study 1 | TNBS3 | Distal | 15.6 | 0.9387 | −0.5 +/− 0.1 |
| | | Proximal | 3.2 | 0.8950 | −2.9 +/− 0.5 |
| | PBS1 | Distal | 7.7 | 0.9851 | −3.3 +/− 0.4 |
| | | Proximal | 1.3 | 0.9274 | −2.7 +/− 0.2 |
| | PBS2 | Distal | 3.5 | 0.9797 | −3.4 +/− 0.4 |
| | | Proximal | 3.8 | 0.9069 | −3.0 +/− 0.1 |
| | PBS3 | Distal | 6.2 | 0.9905 | −2.3 +/− 0.1 |
| | | Proximal | 2.7 | 0.9934 | −2.8 +/− 0.1 |
| | TNBS1 | Distal | 33.8 | 0.9880 | −0.4 +/− 0.1 |
| | | Proximal | 4.5 | 0.9688 | −3.4 +/− 0.1 |
| | TNBS2 | Distal | 58.5 | 0.9745 | −0.3 +/− 0.1 |
| | | Proximal | 6.7 | 0.9763 | −3.3 +/− 0.1 |
| Study 2 | TNBS3 | Distal | 11.4 | 0.9589 | −0.3 +/− 0.1 |